Photoaffinity Labeling of the *Plasmodium falciparum* Chloroquine Resistance Transporter with a Novel Perfluorophenylazido Chloroquine[†]

Jacqueline K. Lekostaj,[‡] Jayakumar K. Natarajan,[§] Michelle F. Paguio,[§] Christian Wolf,[§,||] and Paul D. Roepe*[,‡,§,||,⊥]

Program in Tumor Biology, Department of Chemistry, Department of Biochemistry and Cellular and Molecular Biology, and Center for Infectious Disease, Georgetown University, Washington, D.C. 20057

Received June 5, 2008; Revised Manuscript Received July 24, 2008

ABSTRACT: Several models describing how amino acid substitutions in the *Plasmodium falciparum* chloroquine resistance transporter (PfCRT) confer resistance to chloroquine (CQ) and other antimalarial drugs have been proposed. Further progress requires molecular analysis of interactions between purified reconstituted PfCRT protein and these drugs. We have thus designed and synthesized several perfluorophenyl azido (pfpa) CQ analogues for PfCRT photolabeling studies. One particularly useful probe (AzBCQ) places the pfpa group at the terminal aliphatic N of CQ via a flexible four-carbon ester linker and includes a convenient biotin tag. This probe photolabels PfCRT in situ with high specificity. Using reconstituted proteoliposomes harboring partially purified recombinant PfCRT, we analyze AzBCQ photolabeling versus competition with CQ and other drugs to probe the nature of the CQ binding site. We also inspect how pH, the chemoreversal agent verapamil (VPL), and various amino acid mutations in PfCRT that cause CQ resistance (CQR) affect the efficiency of AzBCQ photolabeling. Upon gel isolation of AzBCQ-labeled PfCRT followed by trypsin digestion and mass spectrometry analysis, we are able to define a single AzBCQ covalent attachment site lying within the digestive vacuolar-disposed loop between putative helices 9 and 10 of PfCRT. Taken together, the data provide important new insight into PfCRT function and, along with previous results, allow us to propose a model for a single CQ binding site in the PfCRT protein.

The gene encoding the *Plasmodium falciparum* chloroquine resistance transporter (PfCRT)[1] was identified by analyzing the progeny of a genetic cross between chloroquine sensitive (CQS) strain HB3 and chloroquine resistant (CQR) strain Dd2 (*1*). Point mutations in the gene that lead to amino acid substitutions in this polytopic integral digestive vacuolar (DV) membrane protein cause chloroquine (CQ) resistance (*1, 2*). Various combinations of amino acid substitutions at 15 different sites in PfCRT are associated with CQR phenotypes, with different substitution patterns originating from various geographic loci and contributing to different "resistance profiles" (rank order resistance to CQ and other drugs). The mechanism by which various PfCRT isoforms confer various drug resistance phenotypes is still unknown, although several hypotheses have been suggested. One such theory proposes that PfCRT acts as a drug efflux pump, using cellular energy to actively translocate CQ from the DV to the cytosol (*3*). Another holds that mutant PfCRT catalyzes facilitative diffusion, allowing charged CQ to passively diffuse out of the DV down its electrochemical gradient (*4, 5*). Versions of either model also incorporate direct (as an ion-coupled symporter) or indirect (secondary to facilitative diffusion function) effects on ion transport, since perturbations in DV pH have been noted for CQR parasites (*6*). Regardless, in all currently favored models, CQ binds to the PfCRT protein.

Tilley and colleagues (*7*) attempted to detect CQ-binding proteins in *P. falciparum* using a radiolabeled azidosalicylate probe and observed labeling of 33 and 42 kDa proteins, with the former later identified as parasite lactate dehydrogenase (*8*). However, these experiments did not quantify competition for probe labeling versus CQ and other drugs and used a probe design that included removing the critical Cl group at position 7 of CQ. Also, they were performed using intact parasite cultures in which the relative abundance of multiple CQ target proteins is unknown but presumably varies widely across the cell (*9*), and well before the identification of PfCRT.

Our laboratory has previously reported the successful heterologous expression of yeast-optimized PfCRT in *Pichia pastoris* (*10*). Using plasma membranes purified from these yeast and equilibrium centrifugation methods, we found that

[†] Supported by NIH Grants RO1 AI056312 and RO1 AI060792 to P.D.R.

* To whom correspondence should be addressed. E-mail: roepep@georgetown.edu. Phone: (202) 687-7300. Fax: (202) 687-7186.

[‡] Program in Tumor Biology.

[§] Department of Chemistry.

[||] Center for Infectious Disease.

[⊥] Department of Biochemistry and Cellular and Molecular Biology.

[1] Abbreviations: PfCRT, *P. falciparum* chloroquine resistance transporter; CQ, chloroquine; pfpa, perfluorophenylazido; AzBCQ, perfluorophenylazido biotinylated chloroquine; VPL, verapamil; CQR, chloroquine resistance (resistant); DV, digestive vacuole; PBS, phosphate-buffered saline; BAD, biotin acceptor domain; PfCRT-h, PfCRT protein with a C-terminal hexa-His tag; PfCRT-hb, PfCRT with both hexa-His and biotin acceptor domain tags at the C-terminus; CM, crude membrane; DM, dodecyl maltoside; PL, proteoliposome; CHCA, α-cyano-4-hydroxycinnaminic acid; QN, quinine; ART, artemisinin; CQS, chloroquine sensitivity (sensitive); QNR, quinine resistance (resistant).

10.1021/bi8010658 CCC: $40.75
Published on Web 09/04/2008

Scheme 1

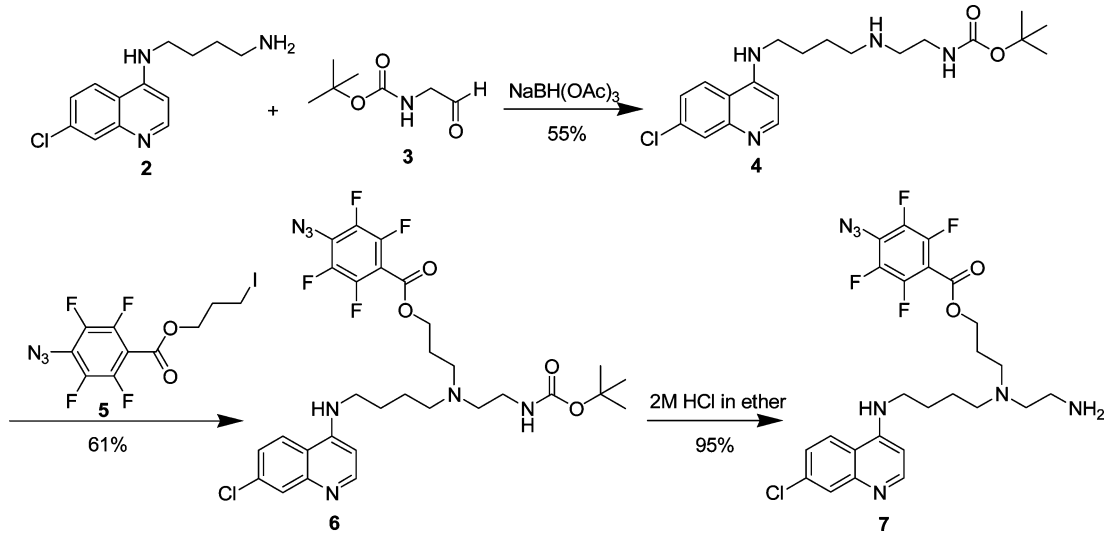

PfCRT binds [^{3}H]CQ (*4*). Small differences in affinity observed for HB3 versus Dd2 PfCRT isoforms (435 nM vs 385 nM) may be caused by the mutations present in Dd2 PfCRT, but the differences measured in ref *4* were not statistically significant. Equilibrium binding experiments are tedious, are expensive, and do not easily allow for routine examination of multiple CQR-associated PfCRT isoforms (i.e., the many geographically distinct isoforms now known to exist) or competition studies with multiple drugs (e.g., determination of the relative affinity for CQ vs other quinoline drugs to which PfCRT confers resistance). The approach also does not provide a way to directly define the drug binding site. We therefore designed CQ photoaffinity analogues that we suspected might have useful properties. One synthesized probe (AzBCQ) adds a perfluorophenylazido (pfpa) moiety to one ethyl group attached to the terminal aliphatic N of CQ via a flexible four-carbon ester linker and also attaches a convenient biotin tag at the other terminal ethyl via a seven-carbon amide linker. Photolabeling strategies have been used to successfully characterize substrate binding to diverse proteins such as the human GLUT4 transporter (*11*), the *Escherichia coli* ATPase SecA (*12*), and proteins involved in malaria-infected RBC adherence (*13*), but none to the best of our knowledge have used pfpa and biotin moieties to rapidly characterize and then map a candidate drug binding site.

MATERIALS AND METHODS

Materials. Monomeric avidin was from Pierce (Rockford, IL). His GraviTrap columns were from Amersham/GE Healthcare (Piscataway, NJ). Float-A-Lyzers were from Spectrum (Rancho Dominguez, CA). Biotinylated molecular weight standards were from Bio-Rad (Hercules, CA). The PentaHis detection kit was from Qiagen (Valencia, CA). The SilverQuest silver stain kit was from Invitrogen (Carlsbad, CA). All other materials were reagent-grade or better and were purchased from Sigma (St. Louis, MO).

Analytical Chemistry Methods. All reagents and solvents were commercially available and used without further purification. Flash chromatography was performed on Kieselgel 60, with a particle size of 0.032−0.063 mm. NMR spectra were recorded on a 300 MHz (^{1}H NMR), 282 MHz (^{19}F NMR), or 75 MHz (^{13}C NMR) Varian FT-NMR spectrometer using $CDCl_3$ as the solvent unless indicated otherwise. Electrospray ionization mass spectra (ESI-MS) were collected on a Thermo Finnigan LCQ instrument. Samples were dissolved in acetonitrile and water (1:1, v/v) containing 1% acetic acid (1 mg/mL) for MS analysis.

Synthesis of Azido-Biotinylated Chloroquine (AzBCQ). 4-Azidotetrafluorobenzoic acid (*14*) and *N*-*t*-Boc-glycinal (*15*) were synthesized by following literature procedures. We first attempted to prepare AzBCQ **1** by the route shown in Scheme 1. Reductive amination of *N*-(7-chloro-4-quinolyl)-1,4-diaminobutane (**2**) and *N*-*t*-Boc-glycinal (**3**) using sodium triacetoxyborohydride produced carbamate **4** in 55% yield. As expected, N-alkylation of **4** with 3-iodopropyl-4-azido-2,3,5,6-tetrafluorobenzoate **5** gave **6** in 61% yield. Removal of the carbamoyl protecting group with 2 M HCl furnished primary amine **7** in 95% yield. However, ^{19}F NMR analysis of the crude amine suggested the presence of two compounds, the expected product **7** and an unidentified byproduct, which is probably a result of HCl-mediated decomposition of the aryl azide via an intermediate aryl nitrenium ion. Efforts to optimize the formation and isolation of **7** were not successful. We therefore developed an alternate strategy for the synthesis of **1**.

This route (Scheme 2) utilizes **4** as the starting material and avoids cleavage of the *t*-Boc protecting group after introduction of the 4-azidotetrafluorobenzoyl moiety. N-Alkylation of **4** with 3-iodo-1-propanol **8** gave alcohol **9** in 62% yield. Removal of the carbamoyl protecting group with 2 M HCl furnished amino alcohol **10** in 97% yield, which was used without further purification. Reaction of **10** and biotin-NHS ester **11** produced biotin-CQ analogue **12** which upon EDC/DMAP coupling with 4-azidotetrafluorobenzoic acid **13** gave AzBCQ derivative **1** in 60% yield. See the Supporting Information for additional details as well as relevant NMR spectra, peak assignments, and HPLC spectra.

Growth and Isolation of Saponin Released Malarial Parasites. P. falciparum strains Dd2 and HB3 were cultured using standard techniques at 2% hematocrit in phenol red free RPMI-1640 (Sigma R8755) supplemented with $NaHCO_3$ (23.8 mM), D-glucose (10 mM), hypoxanthine (730 μM), HEPES (25 mM), gentamicin sulfate (20 μg/mL), and

Scheme 2: Synthetic Schemes for AzBCQ Synthesis

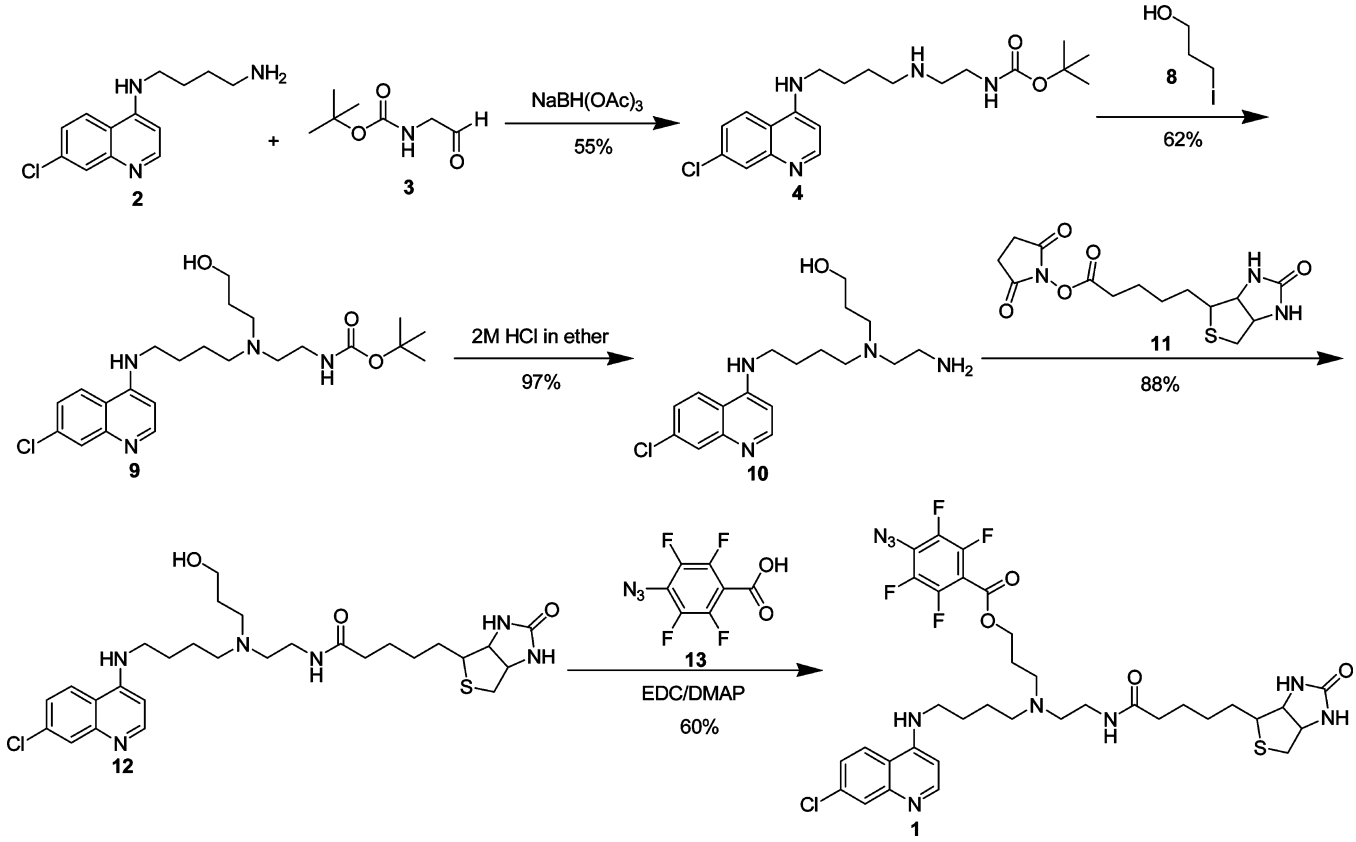

matched human serum (10%). Cultures were triply synchronized with sorbitol (5%, w/v) as described in detail elsewhere (*9, 16*).

A 5 mL iRBC pellet of ~7.5% parasitemia at the trophozoite stage was washed twice in 50 mL of PBS and then resuspended in 50 mL of PBS containing 0.5% (w/v) saponin. The released parasites were collected by centrifugation at 1500*g* for 10 min and then washed twice in 1 mL of ice-cold PBS. The trophozoite pellets were flash-frozen and stored at −80 °C.

Creation and Growth of Yeast Strains. A single clone of the pPIC3.5-crt-bad plasmid from ref *10* was modified to insert sequences encoding a hexahistidine domain and a Factor Xa cleavage site between the *pfcrt* gene and the biotin acceptor domain (BAD). A DNA sequence encoding six consecutive histidine residues (6H) and a Factor Xa recognition sequence (IDGR) was designed as two complementary 45 bp primers with sticky ends simulating NotI- and XmaI-cleaved sites. The primers were annealed and ligated into NotI and XmaI sites of the pPIC3.5-crt-bad plasmid, lying just 5′ to the BAD. After the samples had passed through bacteria, the BAD was then removed from one clone by first replacing the 3′ NotI site with an XmaI sequence via site-directed mutagenesis. Restriction with XmaI then liberated the entire BAD fragment, and the plasmid was recircularized. All results were confirmed by DNA sequencing of the full-length *pfcrt-h* and *pfcrt-hb* genes.

Yeast were transformed either using the LiCl method with 3 μg of linearized target DNA and 50 μg of salmon sperm DNA as a carrier or using the Pichia EasyComp Transformation Kit (Invitrogen) and then plated on minimal dextrose. After being screened for PfCRT expression, the resultant strains were subsequently grown in minimal glycerol medium lacking histidine and protein expression was induced in minimal methanol medium as described previously (*10*).

Purification of Recombinant PfCRT and Reconstitution into Proteoliposomes. Yeast strains transformed with HB3 CRT, Dd2 CRT, 7G8 CRT, or empty vector (pPIC3.5) were grown to an OD_{600} of >2.0 and then induced with minimum methanol medium. PfCRT harboring a C-terminal BAD (*10*) can be purified to near homogeneity via avidin chromatography, whereas purification of PfCRT-His_6 using Ni^{2+} chelating resin in the final step yields partially purified material as described in Results. With either method, at approximately 20 h postinduction, crude membranes (CMs) were isolated as described previously (*17, 18*), and the total membrane protein was quantified by amido black. All subsequent steps were performed at 4 °C. The CMs were diluted to 2 mg/mL in wash buffer [50 mM Tris-HCl, 250 mM sucrose, 20% (v/v) glycerol, and 1 mM $MgCl_2$ (pH 7.5), supplemented with 3 M NaCl] and centrifuged at 100000*g* for 1 h. A loss of 4% protein was assumed on the basis of control experiments, and the washed pellet was resuspended at 2 mg/mL in solubilization buffer (wash buffer supplemented with 500 mM NaCl and 1% DM). After the sample had been gently rotated for 30 min, another 1 h 100000*g* centrifugation was performed. The detergent extract was then applied to a His GraviTrap column (GE) and allowed to flow through. The column was washed with 20 mM imidazole to remove nonspecifically bound proteins, and PfCRT was eluted with 500 mM imidazole. Alternatively, the detergent extract was applied to a column packed with 2 mL of 50% monomeric avidin slurry (Pierce), washed twice with 10 bed volumes of solubilization buffer, and eluted with 6 bed

volumes of elution buffer (solubilization buffer supplemented with 5 mM D-biotin). In either case, the column eluate was immediately mixed with *E. coli* lipid to a final concentration of 1.4% lipid, tumbled gently for 30 min, and then transferred to Float-A-Lyzer dialysis tubing (cutoff of approximately 25000 Da). Dialysis was carried out against ≥50 volumes of buffer [50 mM Tris-HCl, 250 mM sucrose, and 1 mM EDTA (pH 7.5)] for 20 h with one change in buffer after the first 4 h. The dialyzed proteoliposomes were then centrifuged for 1 h at 100000*g*, and the pellet was resuspended in fresh dialysis buffer. Aliquots were snap-frozen and stored at −80 °C.

AzBCQ Photolabeling Reaction. Proteoliposome protein (0.1 nmol) was diluted in 50 mM Mes-Tris at varying pH values (see Results). The solution was aliquoted into wells of a 96-well plate, and appropriate drugs were added as described in Results. All subsequent steps were performed in the dark. The plate was shaken on a MixMate (Eppendorff) at 650 rpm for 30 s and then incubated at 37 °C for 10 min. The plate was then exposed to UV radiation (220−280 nm; 254 nm maximum) from a hand-held lamp (Spectroline model ENF-280C, 115 V, 60 Hz, 200 mA; 8 W bulb emitting approximately 500 μW/cm^2 approximately 10 cm from the bulb surface). The lamp was placed directly upon the plate so that the samples were 0.8 cm from the light source. The reaction was stopped by removing the lamp and mixing equal volumes of the sample with 2× Laemelli buffer. After a 10 min incubation at 37 °C, the samples were divided in half, and equal amounts were loaded onto two 12% SDS−PAGE gels and electrophoresed at 200 V for 1 h at a constant voltage. The proteins were then transferred to two PVDF membranes at 350 mA constant current for 1 h. One membrane was blocked in 10% dry milk (Bio-Rad catalog no. 170-6404) and blotted with streptavidin−HRP conjugate, while the other was developed with the Qiagen PentaHis detection kit according to the manufacturer's instructions.

Densitometry and Normalization. Blots were analyzed using Image J (software available from the National Institutes of Health). The average of at least two intensity values for each PfCRT−AzBCQ band on the biotin blot was divided by that of the corresponding band on the companion polyHis blot as described in Results. Data from at least two pairs of four independent gels are averaged to yield the curves shown in Figures 4−10.

Trypsinization and Mass Spectrometry-Based Identification of PfCRT-Derived Peptides. A large-scale photolabeling reaction was performed essentially as described above. The samples were run in large (100 μL) gel wells with prestained molecular mass ladders (Bio-Rad) on either end. The section of the gel containing PfCRT was excised, minced into ∼1 mm × 1 mm cubes, and transferred to an Eppendorff tube. The gel pieces were then ground using the plunger of a 1 mL syringe as a pestle. Then 1% acetonitrile was added to just cover the acrylamide, and the tube was incubated at 37 °C with vigorous shaking for 1−3 h. The acrylamide bits were pelleted by a short centrifugation at 16000*g*, and the supernatant was removed.

Sequencing-grade trypsin (Sigma) was reconstituted in HPLC-grade water at a concentration of 0.1 μg/μL; 0.5 μg from this stock was activated in 15 μL of 25 mM ammonium bicarbonate, and 10 μL of this mixture (0.25 μg of trypsin) was added to the protein eluted from the gel. The reaction

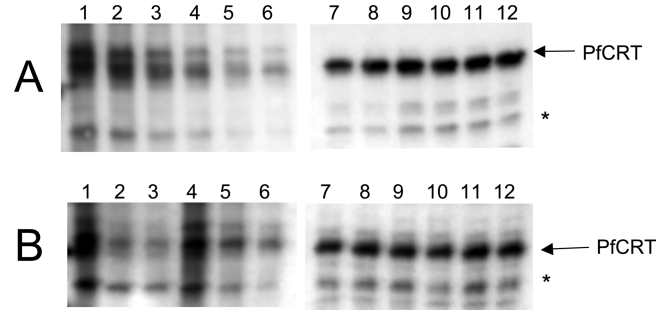

FIGURE 1: AzBCQ labeling of endogenous PfCRT. (A) AzBCQ labeling of saponin-isolated HB3 parasites with 10 μM AzBCQ for 10 min at pH 5.6; from left, competition with cold CQ at 0, 0.8, 1.6, 2.4, 3.2, and 4 mM (lanes 1−6, respectively). Lanes 1−6 are an avidin blot for detecting AzBCQ, and lanes 7−12 show half of the same samples blotted with anti-PfCRT polyclonal antibody. (B) Avidin (lanes 1−6) and anti-PfCRT (lanes 7−12) immunoblots of HB3 and Dd2 saponin-released parasites reacted with 10 μM AzBCQ at pH 5.2 with a 10 min UV illumination time. The arrow indicates the major immunoreactive band on the anti-PfCRT blot. The asterisk indicates a probable degradative byproduct that retains the AzBCQ binding site: lanes 1−3 and 7−9, HB3; lanes 4−6 and 10−12, Dd2; lanes 1, 4, 7, and 10, no competing CQ; lanes 2, 5, 8, and 11, 2 mM CQ competitor; lanes 3, 6, 9, and 12, 4 mM CQ competitor.

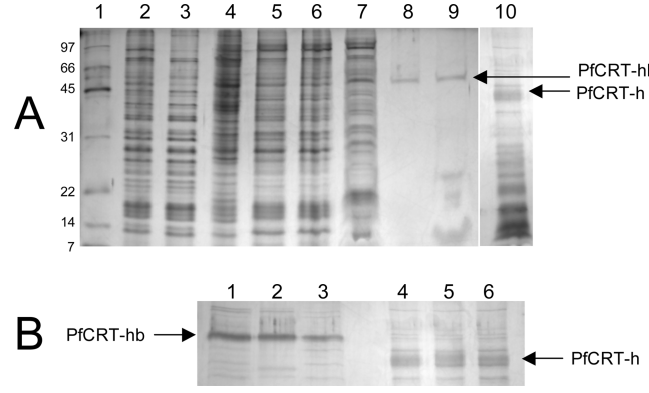

FIGURE 2: Silver staining of membrane fractions and proteoliposomes. PfCRT was partially purified from crude membranes (CMs) and reconstituted into proteoliposomes (PLs). One microgram of protein from various fractions was loaded per lane, and the position of PfCRT-hb or PfCRT-h is indicated by the arrows. (A) Silver staining of purification fractions and comparison of avidin vs nickel chromatography: lane 1, broad range biotinylated molecular mass standards (Bio-Rad); lane 2, HB3 crude membrane; lane 3, supernatant from chaotropic wash; lane 4, residual pellet from detergent solubilization; lane 5, detergent extract; lane 6, column flow through; lane 7, column wash; lane 8, column eluate; lane 9, HB3 proteoliposomes; lane 10, HB3 CRT-His nickel-purified PL. (B) Silver staining of different proteoliposome preparations showing approximately equal yields for different PfCRT isoforms: lanes 1−3, purification by avidin chromatography; lanes 4−6, purification by nickel chromatography; lanes 1 and 4, HB3; lanes 2 and 5, Dd2; lanes 3 and 6, 7G8 PfCRT. Each lane harbored 1 μg of protein.

was allowed to continue at room temperature for various time points as described in Results and was stopped by the addition of 5× Laemelli buffer. The samples were heated at 37 °C for 10 min and run on a 15% acrylamide gel using Tris-glycine buffer. Some gels were silver stained using the MS-compatible SilverQuest kit (Invitrogen), and bands of interest were excised, destained, and further processed for mass spectrometry.

The gel slices were washed with 100 mM ammonium bicarbonate and incubated with 50 mM ammonium bicarbonate and 10 μL of 10 mM DTT at 60 °C for 30 min. The

tubes were cooled to room temperature; 10 μL of 55 mM iodoacetamide was added, and the sample was incubated for an additional 30 min in the dark at room temperature. The solvent was discarded, and the gel slice was washed in 50% acetonitrile and 100 mM ammonium bicarbonate. Subsequently, the gel slice was transferred onto a 96-well Montage plate (Millipore) and destained with 50% acetonitrile in 25 mM ammonium bicarbonate, dehydrated with acetonitrile for 5 min, and vaccuum-dried. Gel pieces were then rehydrated with 15 μL of an ammonium bicarbonate (25 mM)/acetonitrile (10%) mixture supplemented with trypsin (5 ng/μL; Promega, Madison, WI) at 37 °C for 16 h. Tryptic peptides were extracted in a 0.1% TFA/50% acetonitrile mixture and mixed with an equal volume of 5 mg/mL CHCA (Acros Organics). Mass spectra were recorded using a matrix-assisted laser desorption ionization time-of-flight, time-of-flight (MALDI-TOF-TOF) spectrometer (4800 proteomics analyzer, Framingham, MA) set in reflector positive mode by spotting the samples onto a MALDI plate. Samples were ionized with a fixed LASER intensity of 3800 J; 1000 LASER shots were collected per subspectrum and were shot randomly with uniform bias. The detector voltage was 2.1 kV, the bin size set at 0.5 ns, and the signal/noise threshold set at 15. The spectra were collected with a specified mass range of 700−4000 Da and with a focus mass of 2100 Da. Peptide masses were compared with the theoretical masses derived from the sequences for all predicted tryptic peptides (see Results) using the FindPept tool (http://ca.expasy.org/tools/findpept.html), available from ExPASy.

RESULTS

Using the approach depicted in Scheme 2, AzBCQ (**1**) was obtained in good yield (see Materials and Methods and the Supporting Information for a complete description). The essential CQ pharmacophore is preserved within AzBCQ, and the pK_a values of the side chain N and quinolinal N remain unaltered. Both the pfpa and biotin tags are purposefully attached via flexible linkers to the ethyl groups at the very end of the CQ side chain, which can tolerate many structural modifications without a significant loss of drug activity. The attached aryl azide forms a highly reactive nitrene upon UV irradiation, which undergoes efficient C−H bond insertion and thus does not require a free amine on the protein for covalent attachment (*14*). We note that via Scheme 2 the pfpa and biotin groups are attached by linkers whose lengths can be easily modified and that this chemistry can easily be adapted to other quinoline antimalarial drugs.

To test whether AzBCQ binds specifically to the PfCRT protein, we first reacted the probe with isolated midstage trophozoites released from iRBC by saponin treatment as described in Materials and Methods. As shown in Figure 1A, endogenous wild-type (HB3) PfCRT protein (arrow) is efficiently labeled with 10 μM AzBCQ, and "cold" CQ competes with labeling (see the legend of Figure 1). Lanes 1−6 of Figure 1A show avidin−HRP conjugate detection of the AzBCQ probe for samples illuminated in the presence of increasing concentrations of CQ, and lanes 7−12 show a companion anti-PfCRT Western blot of another aliquot of the same samples. Figure 1B compares PfCRT labeling for approximately equal amounts of HB3 (CQS, lanes 1−3 and 7−9) and Dd2 (CQR, lanes 4−6 and 10−12) parasites and

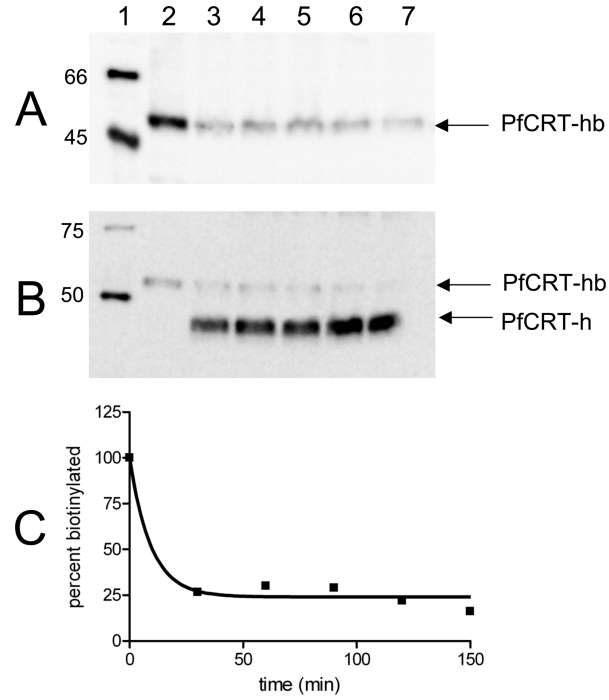

FIGURE 3: Factor Xa digest of CRT-His-BAD PLs to assess topology after reconstitution. (A) Representative avidin and (B) polyHis immunoblots of Dd2 PfCRT-hb digested with Factor Xa: lane 1, biotinylated (A) or polyHis (B) molecular mass standards; lane 2, original undigested PL; lanes 3−7, PL digested for 30, 60, 90, 120, and 150 min, respectively. (C) Plot of the amount of full-length PfCRT-hb remaining over time. Image J (NIH) was used to measure the densitometry of the bands corresponding to PfCRT-hb in the blots in panels A and B. The values were converted to the percent of lane 2, and the results for both blots were averaged; ~76% of the initial protein is cleaved, indicating that at least three-fourths of the molecules are oriented with the C-terminal tail on the outside of the lipid.

shows that CQ competition is qualitatively similar for both isoforms. Again the left side (lanes 1−6) shows avidin−HRP conjugate detection of the biotinylated probe, while the right side (lanes 7−12) shows amounts of PfCRT are similar in all lanes. We note that isolation of saponin-treated parasites routinely yields what we suspect are partially proteolyzed PfCRT fragments (e.g., asterisk) and that some of these apparently include the AzBCQ binding site (compare lanes 1−6 vs lanes 7−12 for Figure 1A, which illustrate bands in both gels at the same position and similar CQ competition for the major vs proteolyzed PfCRT band). Since the epitope for the anti-PfCRT antibody is near the very end of the C-terminus (*1*) and since the major (arrow) and minor (asterisk) bands in Figure 1 differ by approximately 7 kDa, these results suggest approximately 70 amino acids can be removed from the N-terminus of PfCRT without the loss of the AzBCQ covalent attachment site. Other immunoreactive bands may represent proteolyzed PfCRT domains that do not contain the AzBCQ binding site or minor nonspecific reactivity of the polyclonal antibody. Regardless, because recombinant PfCRT protein expressed in yeast is readily available for more detailed analysis (see below) and due to the greater expense of parasite versus yeast culture, we did not explore optimization of this reaction with saponin-released parasites or further fragmentation of labeled endogenous PfCRT by native or exogenous proteases. Photolabeling optimization, drug competition, and proteolysis

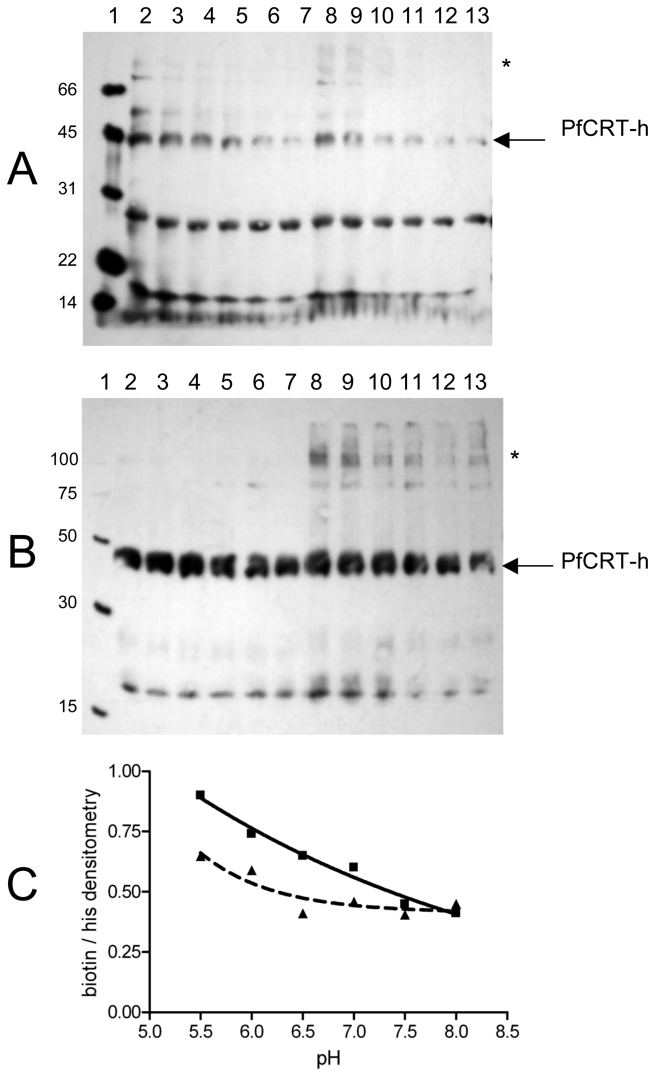

FIGURE 4: Quantitation and AzBCQ labeling of HB3 and Dd2 PfCRT vs pH. Representative avidin−HRP (A) and polyHis−HRP (B) blots of HB3 and Dd2 PfCRT-h PLs photolabeled with 50× AzBCQ at varying pH values with a 10 min UV illumination. The full, uncropped blots are shown, revealing specific binding of the probe despite contaminating proteins in the PLs (see lane 10 of Figure 2A). The band near 16−17 kDa is likely a degradation product of PfCRT. For panels A and B: lane 1, molecular mass standards; lanes 2−7, HB3; lanes 8−13, Dd2; lanes 2 and 8, pH 5.5; lanes 3 and 9, pH 6.0; lanes 4 and 10, pH 6.5; lanes 5 and 11, pH 7.0; lanes 6 and 12, pH 7.5; lanes 7 and 13, pH 8.0. (C) Normalized densitometry obtained by dividing lane intensities in panel A by corresponding lanes in panel B. Results from two pairs of independent gels are averaged to produce the normalized densitometry plot, and two densitometry quantifications were conducted for each set (four in total, standard error of <3% in each case): HB3 (■) and Dd2 (▲).

results are described below for partially purified and reconstituted recombinant PfCRT.

Previously, we reported a partial purification of PfCRT and reconstitution into proteoliposomes (*10*). Figures 2 and 3 show representative results of our further exploration of various purification and reconstitution strategies. As described in Materials and Methods, we have synthesized plasmid constructs in which both a polyHis sequence and a BAD, separated by a Factor Xa protease site, have been added to the C-terminus of PfCRT (PfCRT-hb) and constructs in which only a polyHis tag has been added (PfCRT-h). The former are useful for assessing the topology of reconstituted PfCRT in proteoliposomes and yield a slightly larger but nearly pure PfCRT with a single-step avidin column chromatography purification procedure (Figure 2A, compare lanes 7−9, top arrow). The latter yield recombinant PfCRT of nearly equal mass relative to native but only partial purification with a single nickel chelation chromatography step (second arrow, lane 10). As seen in Figure 2B, with either method, similar yields are obtained for HB3 (CQS; lanes 1 and 4), Dd2 (CQR, VPL reversible; lanes 2 and 5), and 7G8 (CQR, VPL insensitive; lanes 3 and 6) isoforms of recombinant "yeast-optimized" (*10*) PfCRT.

Proteoliposome (PL) suspensions that harbor approximately 1 μg of protein and 100 μg of lipid per microliter are easily prepared from either purified PfCRT-hb or partially purified PfCRT-h. We cannot directly assess the topology of reconstituted PfCRT-h, but Figure 3 shows that reconstituted PfCRT-hb is nearly 80% oriented with the C-terminal region disposed to the outside of the PLs. That is, when these PLs are treated with Factor Xa to cleave the BAD from the rest of the protein, the avidin−HRP reactive species that migrates near 52 kDa (Figure 3A, top band in Figure 3B) disappears and is converted to PfCRT-h that migrates at 47 kDa (bottom band in Figure 3B, lanes 3−7). Interestingly, the polyHis epitope inserted N-terminal to the BAD in PfCRT-hb is much less reactive with respect to anti-His antibody than when it is "liberated" upon removal of the BAD by Factor Xa (compare lanes 2 and 3 of Figure 3B, which have the same total amount of PfCRT protein). Integrating intensities of the PfCRT-hb and PfCRT-h bands show that approximately 75% of the biotin acceptor domain is cleaved by Factor Xa in 30 min (Figure 3C). Since Factor Xa cannot penetrate to the interior of these well-sealed PLs, this indicates that the majority of PfCRT is reconstituted with the C-terminus disposed outward, which corresponds to the predicted topology for PfCRT within the native DV membrane (*1*).

With PfCRT-h versions of these PLs in hand, we then optimized photolabeling conditions to quantitatively test competition between AzBCQ and other drugs. Our methodology in these quantitative experiments is shown in Figure 4. Lanes 2−13 in Figure 4A show AzBCQ binding to HB3 (2−7) and Dd2 (8−13) isoforms of PfCRT-h versus pH (see the legend), and the corresponding lanes in Figure 4B show another aliquot of the same samples run on a separate gel and probed with an anti-pentaHis-HRP antibody after electrophoretic transfer. We used PfCRT-h PLs in these experiments for two reasons. First, the BAD attached to PfCRT-hb would obviously compete for avidin−HRP conjugate detection of the biotin moiety attached to AzBCQ, making quantification impossible (residual BAD biotin would remain even after Factor Xa cleavage; cf. Figure 3). Second, even though the PfCRT-h PLs that we are able to fabricate with current procedures contain only partially purified PfCRT (lane 10 vs lane 9 of Figure 2A), we felt that the presence of a number of contaminants represented an opportunity to gauge the specificity of the photolabeling reaction. This means that if reaction conditions were too robust, additional cross-linking to contaminants would be seen for PfCRT-h PLs whereas if the conditions generated PfCRT-h specific binding, a single band would be observed. Also, fortuitously, a naturally biotinylated yeast protein contaminant is carried through via the nickel chelation purification strategy (Figure

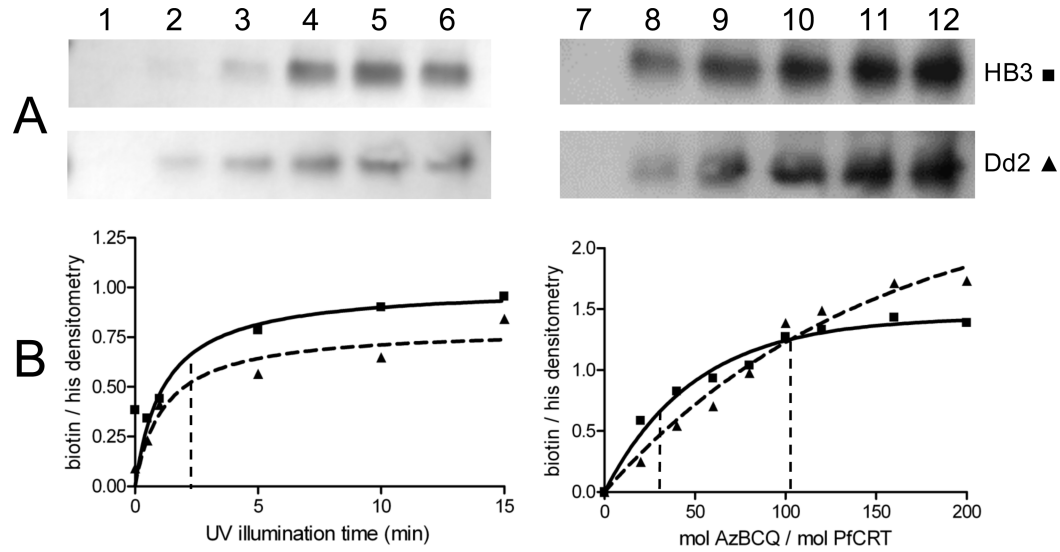

FIGURE 5: AzBCQ labeling of HB3 and Dd2 PfCRT as a function of UV illumination time and probe concentration. Representative avidin blot strips (A) and normalized densitometry (B) of AzBCQ photolabeling of HB3 (■) and Dd2 (▲) at varying UV illumination times (left-hand side) and mole ratios of AzBCQ to PfCRT (right-hand side). When the time was varied, measurements were taken at a 50-fold molar excess of AzBCQ relative to PfCRT. For panel A (left-hand side): lane 1, 0 min; lane 2, 30 s; lane 3, 1 min; lane 4, 5 min; lane 5, 10 min; lane 6, 15 min. Each data point in panel B is the average of at least two independent experiments, and two densitometry quantifications were conducted for each gel. Half-maximal labeling vs time is denoted with the vertical dashed line (B, left-hand side). Representative avidin−HRP conjugate blot (A, right-hand side) and normalized densitometry (B, right-hand side) of HB3 and Dd2 PfCRT photolabeled with increasing amounts of AzBCQ and a 10 min UV illumination. In panel A (right-hand side), lane 7 contained no AzBCQ and lanes 8−12 contained 20-, 40-, 60-, 80-, and 100-fold molar excesses of AzBCQ, respectively. In panel B (right-hand side), we show saturation of AzBCQ photolabeling at a fixed illumination time. Each point is the average of at least two independent determinations. Half-maximal photolabeling occurs at 34- and 102-fold molar excesses of AzBCQ for the HB3 and Dd2 isoforms, respectively (first and second vertical dashed lines), as determined using the equation $Y = Y_{max}(1 - e^{-Kx})$ (solid and dashed lines, respectively).

4A, second band migrating near 30 kDa). This band provides convenient verification in avidin−HRP conjugate blots (e.g., Figure 4A) that equal amounts of AzBCQ-reacted PfCRT-h PLs are loaded in each lane. Figure 4B confirms this, by showing the results of a companion anti-His-HRP Western blot using another aliquot of the same samples run in each of the corresponding lanes of the blot shown in Figure 4A. Although outside the scope of the experiments summarized in this paper, we note that frequently the labeled Dd2 isoform of PfCRT also migrates at a higher mass, corresponding to that predicted for a dimer (asterisk, lanes 7−12 of Figure 4B), under conditions where the HB3 isoform does not. Intensities of dimer bands were not included in the quantification of photolabeling efficiency as described below.

When the intensities of the monomeric PfCRT bands in Figure 4B are divided into those for the corresponding bands in Figure 4A and the results of two independent experiments (two independent photolabeling reactions, four gels, four Western blots, and eight independent densitometry calculations) are averaged and plotted (Figure 4C), relative AzBCQ photolabeling versus pH for the two isoforms is quantified. We find there is a stronger pH dependence for photolabeling of HB3 (CQS) PfCRT-h (■) than for Dd2 (CQR) (▲). We note that, formally, this altered pH dependency reveals either different pH-dependent probe binding for the two isoforms or altered pH dependency of the photolabeling reaction that culminates in covalent attachment of the probe to PfCRT. However, since the probe is exceedingly reactive and since strong effects of pH on that chemistry are not expected (*14*), the former is more likely.

Using this methodology (Figure 4), we then quantified the effects of important photolabeling reaction parameters. Namely, efficiencies of labeling versus illumination time and versus various AzBCQ:PfCRT mole ratios (Figure 5, left- and right-hand sides, respectively) were determined for HB3 and Dd2 PfCRT. Half-maximal labeling was achieved within 2−3 min (Figure 5, left) of UV exposure at a range of AzBCQ concentrations. Titrating AzBCQ into a fixed amount of PfCRT PLs (Figure 5, right) showed half-maximal labeling after illumination for 10 min at molar ratios (AzBCQ:PfCRT) of approximately 34 and 102 for the HB3 and Dd2 isoforms, respectively (Figure 5B, right-hand side, first and second vertical dashed lines, respectively). Although photolabeling efficiencies of probes that are believed to be specific to transporters or channels vary widely, [e.g., (19−22)], these results are at the lower end of the range of apparent affinities for azido drug probes and suggest that AzBCQ photolabeling of PfCRT is quite efficient and specific. Using known amounts of biotinylated protein standards (e.g., lane 1 of Figure 4A) and quantitation of the purified PfCRT protein, we estimate that the stoichiometry of labeling is 0.14 mol of AzBCQ/mol of PfCRT when the illumination time is fixed at 10 min and the molar ratio of AzBCQ to PfCRT in the reaction is set at 50. Since the stoichiometry is less than 1:1, this again suggests (but does not prove) that photolabeling under these early plateau conditions is quite specific and involves a single drug binding site.

Using these conditions and using the methodology described in the legend of Figure 4, we then quantitatively compared the pH dependency of AzBCQ photolabeling (Figure 6) and competition versus other drugs (Figure 7) for HB3, Dd2, and 7G8 PfCRT isoforms. Interestingly, at pH 5.0, both CQR-conferring isoforms (Dd2 and 7G8) are less efficiently labeled than the HB3 (CQS) isoform (Figure 6A, lane 1). However, we note that in our hands, live intraerythrocytic parasites harboring Dd2 or 7G8 isoforms have DV

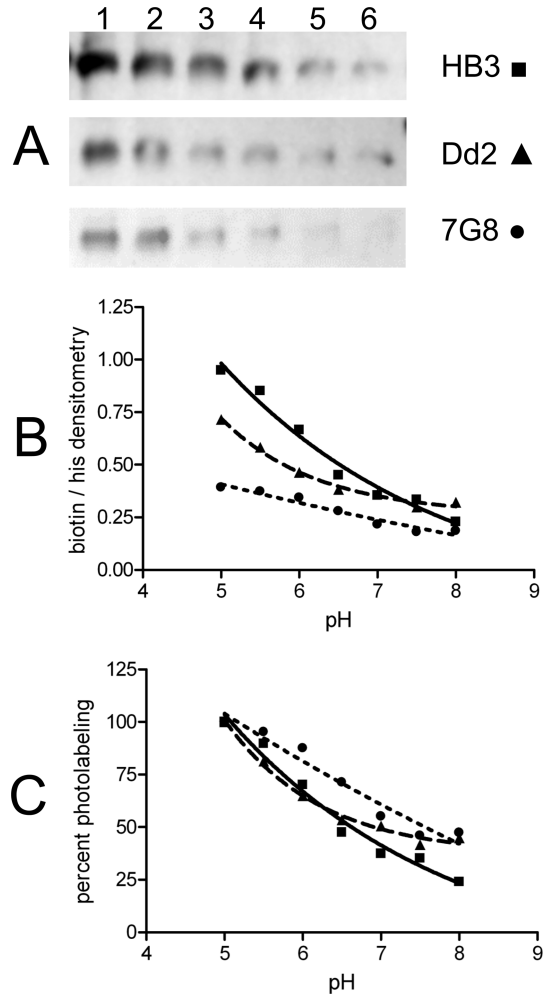

FIGURE 6: Quantitation of labeling vs pH for multiple PfCRT isoforms. Representative avidin blot (A) and normalized densitometry of absolute (B) and percent (C) AzBCQ labeling of HB3 (■), Dd2 (▲), and 7G8 (●) at various pH values. AzBCQ was present in a 50-fold molar excess relative to protein, and the UV illumination time was 10 min. Each data point is the average of at least two independent experiments, and two densitometry quantifications were conducted for each set of gels (four in total, standard error of <3% in each case). For panel A: lane 1, pH 5.5; lane 2, pH 6.0; lane 3, pH 6.5; lane 4, pH 7.0; lane 5, pH 7.5; lane 6, pH 8.0.

pH values 0.4−0.5 unit lower than that of HB3 (*6*); thus, these data suggest that, in vivo, drug binding to Dd2 PfCRT may be more similar to that of HB3 PfCRT. Since the absolute efficiency of photolabeling is a function of several variables, we plot both absolute densitometry results for the three isoforms (panel B) as well as percent labeling, normalized to the maximal labeling for each isoform (panel C).

Competition for AzBCQ photolabeling by increasing concentrations of cold CQ (Figure 7, left-hand side) again argues that the probe is quite specific. Under standard labeling conditions, half-maximal CQ competition is achieved at 22-, 25-, and 6-fold molar ratios (CQ:AzBCQ) for the HB3, Dd2, and 7G8 isoforms, respectively. This very impressive CQ competition strongly suggests (but does not prove) that the binding sites for AzBCQ and CQ overlap. A less likely possibility is that binding of one allosterically regulates binding of the other. If we assume the binding sites overlap, the data also suggest that the 7G8 isoform has increased affinity for CQ relative to the other two isoforms. Also, although the range of successful competition ratios of "cold" drug substrate versus azido drug probes varies widely in the literature, we note these CQ:AzBCQ ratios are very much at the low end of the range, particularly for 7G8. For example, efficient competition for azido analogues of vinblastine (VBL) or verapamil (VPL) that photolabel human P-glycoprotein is seen at approximately 200−10000-fold molar excesses of cold VBL or cold VPL versus the corresponding azido derivatives (*19*−*21*).

Figure 7 (middle) shows similar results for competition using the related quinoline antimalarial drug QN. Here, competition seems to be more similar for the three isoforms, with half-maximal competition at 19-, 16-, and 10-fold molar excesses (QN:AzBCQ) for HB3, Dd2, and 7G8 isoforms, respectively. In contrast, Figure 7 (right-hand side) shows that the non-quinoline antimalarial drug artemisinin (ART) does not efficiently compete for AzBCQ photolabeling. In fact, there appears to be a subtle yet reproducible increase in the level of AzBCQ photolabeling for the resistance-conferring isoforms (Dd2 and 7G8) upon addition of an increasing concentration of ART.

Figure 8 summarizes particularly interesting results with the chemoreversal agent verapamil (VPL). Half-maximal competition of AzBCQ photolabeling is achieved at 35- and 40-fold molar excesses of VPL for HB3 and Dd2 PfCRT, respectively, suggesting that VPL and AzBCQ binding sites overlap and that the affinity for VPL is similar for these two isoforms. However, no competition is seen in the case of the 7G8 isoform. Perhaps not coincidentally, the 7G8 isoform is expressed in CQR parasites that are resistant to chemosensitization by VPL. In fact, similar to ART, a small but reproducible increase in the level of AzBCQ labeling is seen for 7G8 PfCRT in the presence of VPL.

The data described above taken together indicated to us that localization of the AzBCQ binding site by proteolysis and mass spectrometry-based identification of labeled peptide(s) was warranted. Figure 9A shows that AzBCQ-labeled HB3 PfCRT can be efficiently cleaved by trypsin to produce an approximately 17 kDa band that remains biotinylated (AzBCQ is bound; lane 3) and that is also immunoreactive to anti-His antibody (arrow, lane 6). The full-length labeled protein (47 kDa) appears to be trypsinized predominantly to a 33 kDa fragment, and then to 17 kDa. Subsequent digestion did not allow us to resolve smaller labeled fragments, although a 7 kDa unlabeled and non-anti-His reactive fragment was identified on companion silver-stained gels (data not shown). Therefore, the 17 kDa band was excised from a destained gel and trypsinized overnight within the gel fragment (see Materials and Methods), and the eluted tryptic peptides were injected into a MALDI-TOF-TOF mass spectrometer.

Upon UV activation, the pfpa group of AzBCQ is predicted to insert at one or more C−H bonds (*14*) and in the process will liberate two nitrogens from the azido moiety. That is, the stable adduct will add 766.25 Da to the mass of any peptide containing an amino acid to which AzBCQ is attached. Subtraction of 766.25 Da from the masses of all peaks displayed in the peptide *m*/*z* spectrum (not shown) yielded one and only one peak that corresponds to a predicted tryptic fragment residing with the 17 kDa C-terminal region of HB3 PfCRT. That peak is at *m*/*z* 2024.64, which is within

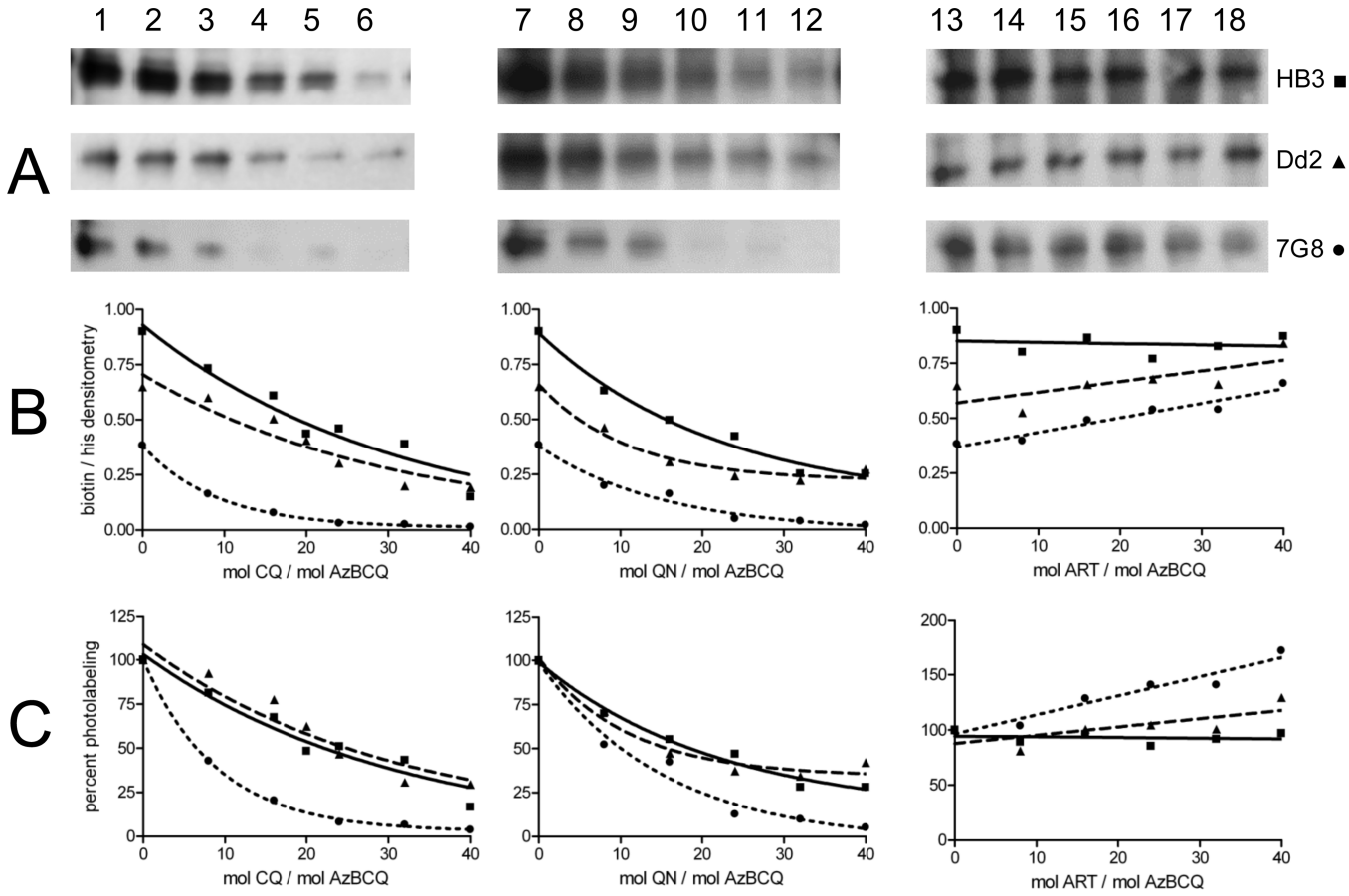

FIGURE 7: Competition of AzBCQ labeling of HB3, Dd2, and 7G8 PfCRT by CQ (left), QN (middle), and Art (right). AzBCQ labeling of HB3 (■), Dd2 (▲), and 7G8 (●) PfCRT labeling at varying drug:AzBCQ ratios (*x* axes in panels B and C). AzBCQ was present in a 50-fold molar excess relative to protein, and the UV illumination time was 10 min. Each data point in panels B and C is the average of at least two independent experiments, and two densitometry quantifications were conducted for each set of gels (four in total, standard error of <3% in each case). For representative avidin blot strips (A) the top strip in each case is HB3, the middle Dd2, and the bottom 7G8: lane 1, no CQ; lanes 2−6, 8-, 16-, 24-, 32-, and 40-fold excesses of CQ relative to AzBCQ, respectively; lane 7, no QN competitor; lanes 8−12, 8-, 16-, 24-, 32-, and 40-fold excesses of QN relative to AzBCQ, respectively; lane 13, no ART competitor; lanes 14−18, 8-, 16-, 24-, 32-, and 40-fold excesses of ART relative to AzBCQ, respectively.

0.30 Da of that for the peptide defined by residues 364−374 (Figure 9B, bold). These residues are believed to comprise the intradigestive vacuolar loop connecting putative helices 9 and 10 (Figure 9B, underlined) of PfCRT protein. A non-AzBCQ-labeled peptide peak was also found in the spectrum that is within 0.16 Da of the predicted trypsin product $E_{372}P_{373}R_{374}$, suggesting that AzBCQ is bound at a single residue within the sequence F_{364}LAGDVVR_{371}. However, we note that the sequence EPR is also a predicted tryptic peptide for human keratin, which is a common contaminant in MS peptide identification. Regardless, on the basis of this definition of the AzBCQ binding site, the impressive isoform specific competition for AzBCQ photolabeling described above, and previous results from us and others reviewed in Discussion, we propose that the AzBCQ (CQ) binding site in PfCRT includes a pocket formed by helices 1, 9, and 10 as shown in cartoon form in Figure 10.

DISCUSSION

In this study, we have synthesized a perfluoroazido, biotinylated chloroquine analogue we name AzBCQ and have analyzed the reactivity of that probe versus endogenous and recombinant, partially purified PfCRT protein. We have quantified the pH dependency of photolabeling for multiple PfCRT isoforms [CQS, CQR-conferring/VPL sensitive (Dd2), and CQR-conferring/VPL insensitive (7G8)] and have quantified quite impressive competition by CQ. We also quantify competition by QN, ART, and VPL under fixed early plateau conditions. We have determined that there is a single covalent attachment site for AzBCQ within the C-terminal tail region of PfCRT and have mapped the site for HB3 PfCRT to 8−11 residues that define the predicted loop between putative helices 9 and 10 of the PfCRT protein.

Photolabeling of transporters, channels, or receptors with azido substrate analogues is a well-known approach for defining substrate binding and mapping binding site domains. Perfluoroazido probes have not been used as extensively as other azido moieties but nonetheless have proven to be quite valuable (e.g., refs *23* and *24*). To the best of our knowledge, only a handful of studies have engineered nonradioactive, biotinylated, azido probes for labeling studies (e.g., refs *25* and *26*) and none have incorporated use of the more reactive perfluoroazidophenyl group, which upon UV illumination efficiently inserts at a C−H bond and so is more versatile than the azidophenyl group (*14*). In some situations, the combined pfpa−biotin tag approach may be quite useful and versatile, allowing for a variety of convenient strategies for rapidly characterizing probe binding.

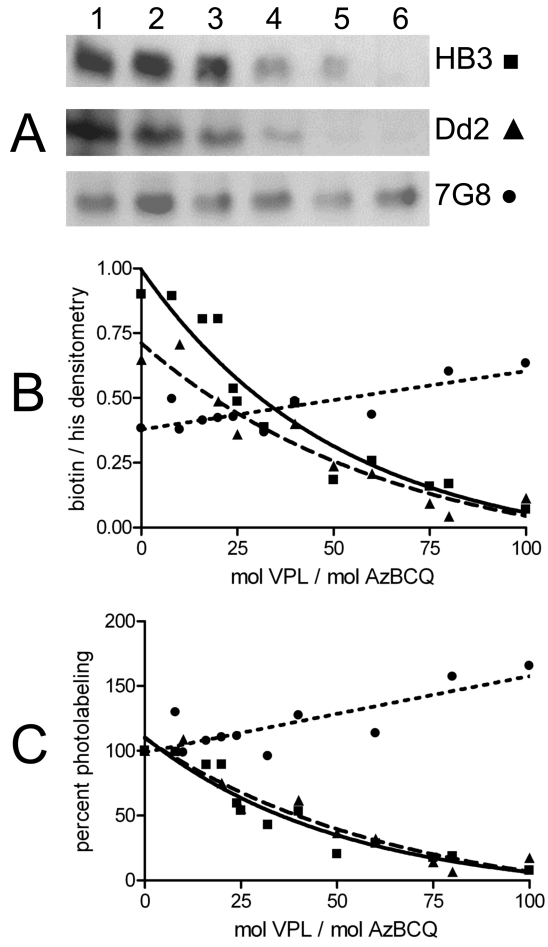

FIGURE 8: Competition of AzBCQ labeling of HB3 and Dd2 PfCRT with VPL. AzBCQ labeling of HB3 (■), Dd2 (▲), and 7G8 (●) at varying VPL:AzBCQ molar ratios. AzBCQ was present in a 50-fold molar excess relative to protein, and the UV illumination time was 10 min. Each data point in panels B and C is the average of at least two independent experiments, and two densitometry quantifications were conducted for each set of gels (four in total, standard error of <3% in each case). For avidin blots in panel A: lane 1, no VPL competitor; lanes 2−6, 8-, 16-, 24-, 32-, and 40-fold excess of VPL relative to AzBCQ, respectively.

Previously, Tilley and colleagues (*7*) used a ^{125}I-labeled azidosalicylate CQ analogue in an attempt to identify CQ binding proteins in *P. falciparum*. Aside from using azidophenyl instead of pfpa, the probe synthesis also required loss of the Cl atom at position 7 of the CQ pharmacophore. We now know that the Cl atom is crucial for full activity of the 4-aminoquinoline, so some differences in our results versus those in ref *7* are to be expected; this might also explain why the earlier probe did not label proteins with a mass equal to that of PfCRT. In addition, the photoactivatable group used in ref *7* was attached to the quinoline ring system, not to the end of the CQ side chain via flexible linkers. On the basis of the AzBCQ binding site mapping we are now able to do (described below), this bulky addition to the quinoline ring system pharmacophore would be predicted to negatively affect binding of the pharmacophore to intrahelical domains of PfCRT. In contrast, the pfpa and biotin tags we engineer are attached by flexible linkers and are predicted to extend out into the extramembranous space (Figure 10) where they would not impede docking of the "CQ portion" of AzBCQ to the proposed CQ binding site. This might explain why competition of AzBCQ photolabeling with CQ, QN, and VPL that we measure is so impressive; essentially, the flexible tags attached to the CQ chain termini do not interfere with pharmacophore docking.

It is tempting to correlate photolabeling efficiencies for the different PfCRT isoforms with binding affinities (meaning, more efficient photolabeling indicates more efficient binding). However, this is overly simplistic since environmental effects that are unrelated to probe affinity can also influence the net efficiency of the photolabeling reaction. Nonetheless, quantifying competition of the photolabeling reaction under early plateau conditions, where labeling is just beginning to saturate, likely yields relative affinities for a competitor, assuming the binding sites for probe and competitor overlap. On the basis of calculated stoichiometries here and in ref *4* and the extremely efficient competition of CQ for the AzBCQ reaction versus all three PfCRT isoforms, it seems reasonable to suggest that this single AzBCQ binding site and a single CQ binding site overlap for PfCRT. Results with 7G8 PfCRT are particularly impressive. We can find no examples of efficient drug probe competition in the literature that are anywhere near 6-fold. In fact, as mentioned, when competition has been carefully quantified previously for drug receptors (e.g., ion channels to which a drug binds with high affinity) or putative drug transporters (e.g., human P-glycoprotein), effective competition is not typically seen until a >200-fold molar excess of the cold drug relative to drug probe is reached. Competition by CQ at low molar excesses suggests that AzBCQ photolabeling is mimicking physiologically relevant binding of CQ to the PfCRT isoforms.

Other evidence, when taken together, strongly supports this notion. (1) Most dramatically, a single attachment site for the probe is mapped to residues 364−374 and is likely to lie within the $F_{364}-R_{371}$ segment. This loop is predicted by multiple algorithms (*1*) to reside within the DV environment, which is known to have an acidic pH between 5.2 and 5.6, depending on whether the parasite is CQR or CQS (*6*). (2) Not coincidentally then, binding of AzBCQ appears to be strongly activated by an acidic pH that corresponds to that predicted for the DV interior (Figure 6). (3) Relatedly, we note initial equilibrium binding studies with [^{3}H]CQ (*4*) calculated a K_d that corresponded to concentrations of CQ that are only predicted for the interior of the acidic DV and that are far higher than concentrations predicted for the cytosol. That is, all predictions from previous equilibrium binding studies (*4*) are entirely consistent with the AzBCQ photolabeling that we measure. Taking these observations together, one obvious conclusion is that AzBCQ binding is indeed mimicking physiologic CQ binding at an acidic, DV-disposed binding site that is in part defined by the helix 9−helix 10 domain.

The loop connecting helices 9 and 10, to which AzBCQ is found covalently attached, is predicted by multiple algorithms to lie within the DV interior (*1*). Again perhaps not coincidentally, residue 371 lying within this loop is mutated in a number of well-known CQR *P. falciparum* strains and isolates, including Dd2, W2, FCB, 2300 (Indonesia), and 742 (Cambodia). Poorly understood patterns of mutations that include other nearby residues, 356 (helix 9), 326 (helix 8), and 271 (loop 7), are also found in most known CQR strains and isolates. On the basis of predicted models for PfCRT function (*1, 4, 5*), it is logical to assume that

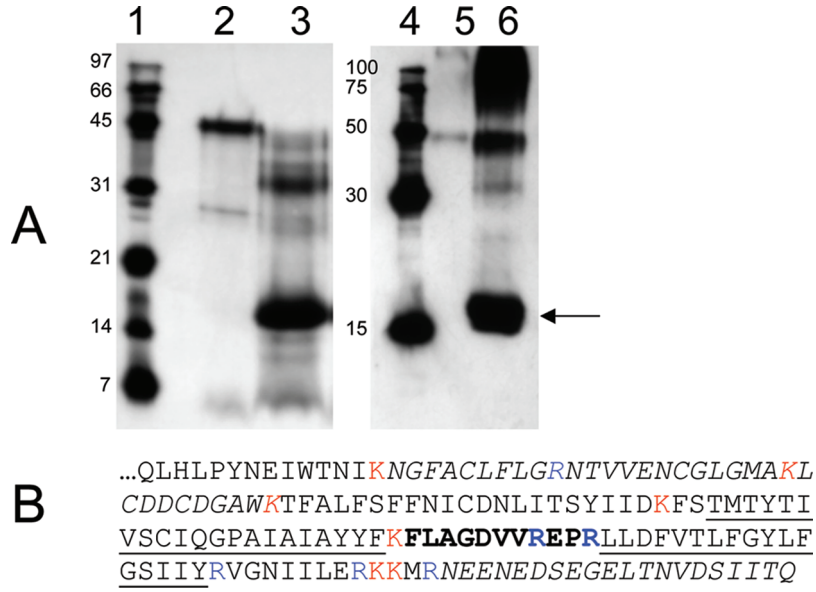

FIGURE 9: Trypsin digestion and mass spectrometry identification of the AzBCQ attachment site. (A) Avidin blot (left) and polyHis blot (right) of HB3 PfCRT-h reacted with AzBCQ and then digested with trypsin: lanes 1 and 4, molecular mass standards; lanes 2 and 5, undigested full-length HB3 PfCRT-h; lanes 3 and 6, PfCRT-h digested with trypsin as described in Materials and Methods. The indicated band (arrow; the smallest band we could identify which contained both the AzBCQ and the polyHis tags) was excised from the gel and further digested to completion with trypsin, and the fragments were resolved by MS as described. (B) C-Terminal PfCRT sequence (amino acids 271−424) corresponding to the last 18.6 kDa of the protein. K and R trypsin sites are colored (trypsin acts C-terminal to K and R residues). Transmembrane helices 9 and 10 are underlined. The AzBCQ binding site is in bold. As described in the text, peaks from MS analysis of an approximately 17 kDa gel-excised band were analyzed for amino acid composition. Peptides corresponding to unmodified amino acids 285−317 (NGFACLFLGRNTVVENCGLGMAKLCDDCDGAWK) and 405−424 (NEENEDSEGELTNVDSIITQ) (italics) were easily identified by MS and correspond to predicted tryptic peptides. Additionally, one low-mass peak corresponding to the tripeptide "EPR" could have originated either from PfCRT amino acids 372−374 or perhaps from a keratin contaminant. Since masses of these C-terminal tryptic peptides correspond to MS peaks ± 0.5 Da, these fragments cannot contain a covalently attached AzBCQ. Upon UV activation, the AzBCQ molecule loses N_2 and inserts at nearby C−H bond(s), resulting in an adduct that would add 766.25 Da to a tryptic peptide within this C-terminal region; 766.25 was therefore subtracted from the peaks obtained in the mass spectrum, and those values were compared to those of all predicted tryptic fragments in the C-terminal region. One and only one hit was obtained, which corresponded to the 11-amino acid stretch (FLAGDVVREPR, in bold) located between TM9 and TM10 (underlined). AzBCQ must therefore be attached to one of these amino acids. As mentioned, the EPR fragment may correspond to an unlabeled PfCRT fragment, which would further narrow the possible positions for the label to amino acids within the FLAGDVVR sequence.

mutations in PfCRT associated with CQR might cluster within or near a CQ binding site.

Another line of evidence that strongly supports the conclusion that AzBCQ photolabeling is mimicking physiologically meaningful CQ binding comes from the recent elegant studies of Cooper et al. (*27*). In these studies, "second site suppressor" mutations were found when pressuring Sudan 106/1-derived CQR clones harboring K76I mutations with QN. These clones had been unusually sensitive to QN but upon selection with the drug became QNR and concomitantly reacquired sensitivity to CQ. The suppressor site was found to be Q352; introduction of a positive charge (either K or R) at this residue conferred the unusual QNR/CQS phenotype to K76I clones. The authors interpreted these results to suggest that putative helix 9 (within which Q352 is predicted to lie; see the asterisk and legend of Figure 10) participates with helix 1 [site of the well-known K76T, K76I, and K76N mutations that confer CQR (*1, 27*); see the asterisk and legend of Figure 10] to form a quinoline drug binding pocket. Our results with AzBCQ strongly support this hypothesis.

By finding that the single attachment site for AzBCQ lies within residues F_{364}−R_{371}, and knowing the geometry and size of the AzBCQ molecule (Figure 10), we suggest that helix 10 must also form part of the binding pocket. Other drug selection results suggest some possible interaction between drugs and helix 4 (*27*), but we are unable to construct a viable model that places helices 1, 9, and 10, loop 9 (the loop between helices 9 and 10), and helix 4 together to form one CQ pocket such that PfCRT residues found to be mutated in CQR are proximal to the CQ pharmacophore within AzBCQ and that allows for attachment of AzBCQ to loop 9. It may be possible that multiple PfCRT conformations exist and that CQ (or other quinoline) binding biases toward one conformation over another. Additional studies with AzBCQ and similar probes with altered geometries may be able to test this idea.

We note that the requirement for larger amounts of VPL to compete away label (relative to CQ) is consistent with the need for relatively high VPL concentrations (1−2 μM) for chemoreversal in culture. The fact that AzBCQ binding to Dd2 PfCRT (found in VPL reversible CQR strains) is efficiently reversed by similar levels of VPL but 7G8 PfCRT (found in VPL insensitive CQR strains) is not is again very strong evidence that the binding site revealed by AzBCQ photolabeling is physiologically relevant. Also, it is very interesting that VPL also efficiently competes for AzBCQ labeling to HB3 PfCRT. It seems reasonable to suggest that mutations which distinguish Dd2 from HB3 may not be relevant for VPL binding but that mutations that distinguish the 7G8 isoform from both the HB3 and Dd2 isoforms destroy the VPL binding site. These are 72S, 326D, and 356L. Again, perhaps not coincidentally, two of these are near the AzBCQ attachment site that we map, and all three

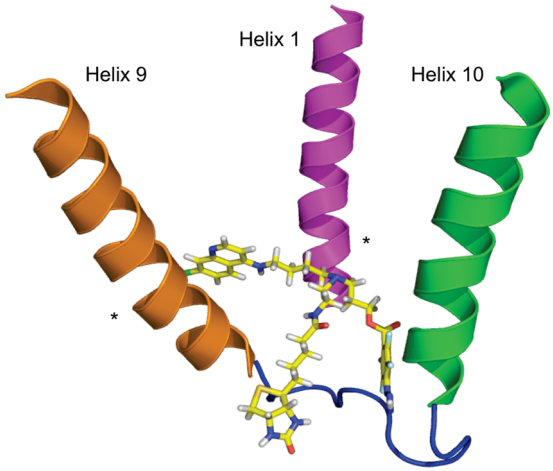

FIGURE 10: Cartoon model for the AzBCQ (CQ) binding site within PfCRT protein. On the basis of these and previous results, we propose that the AzBCQ 7-chloro-4-aminoquinoline pharmacophore (i.e., the CQ pharmacophore) binds within a cleft defined by helices 1 (purple), 9 (brown), and 10 (green) such that residues in helices 1 and 9 mutated in CQR vs CQS isoforms of PfCRT (near the asterisk) are proximal to the pharmacophore. This geometry easily permits the defined covalent attachment site within the loop between helices 9 and 10 (blue line) to contact the perfluoroazido side chain of the probe without disrupting predicted pharmacophore−helix interactions. Also, this geometry allows the biotin tag to be easily accessible outside the membrane in which the helices are imbedded. Notably, the model easily provides for a number of possible contacts between helix 1-mutated residues (near the asterisk, helix 1) and helix 9-mutated residues (near the asterisk, helix 9) as described in Discussion. Also, the model explains impressive isoform specific CQ, QN, and VPL competition, as flexible pfpa- and biotin-tagged side chains do not occupy the intrahelical CQ binding site but instead extend into the aqueous space. AzBCQ coordinates were computed with MM2, and the helices were built on the basis of the structure of the acetylcholine receptor m2 transmembrane segment (PDB entry 1EQ8). The AzBCQ molecule was manually docked onto the built helices using PyMOL (Delano Scientific LLC).

lie within or near the CQ binding pocket that we propose on the basis of these data.

It is surprising to us that HB3 PfCRT more strongly binds AzBCQ under basal conditions than Dd2 and 7G8 isoforms do and that VPL and CQ competition for AzBCQ photolabeling is quite similar for HB3 and Dd2 PfCRT isoforms [half-maximal competition at 35- and 40-fold (VPL) and 22- and 25-fold (CQ) molar excesses, respectively]. Thus, unlike the case for 7G8 PfCRT, and not withstanding the caveats noted above regarding the dangers of correlating photolabeling versus binding, Dd2 mutations likely do not significantly alter HB3 PfCRT drug affinity. This is also perfectly consistent with our earlier equilibrium binding results with [^{3}H]CQ which measured K_d values of 385 and 435 nM for the Dd2 and HB3 PfCRT isoforms, respectively (*4*). Dd2 mutations must therefore confer other functions to PfCRT that confer CQR and that remain to be molecularly defined (*4, 5*).

Finally, a note of caution mixed with speculation regarding these other functions of PfCRT. Photolabeling efficiencies are a product of probe binding and the chemical environment within which the photochemistry is generated. The attachment site we identify is within a loop disposed outside of the membrane. This suggests that we can be reasonably confident the chemical environment near the reactive pfpa group is similar for all three isoforms (e.g., extramembranous and aqueous). This observation along with noting the highly reactive nature of the pfpa group suggests photolabeling differences for the PfCRT isoforms likely reflect different binding affinities of the pharmacophore. These will be the product of on versus off rates for the probe. On the basis of the pH dependence of labeling, this then leads us to speculate that pH either increases the CQ off rate or decreases the CQ on rate for Dd2 and 7G8 versus HB3. The former is indirect support for mutant PfCRT acting as a pH-dependent facilitative CQ transporter (perhaps a channel specific to CQ^{2+}), which has been proposed by us (*4*) and others (*5*). These points and many others obviously merit detailed inspection via additional PL experiments with AzBCQ and other molecular probes.

ACKNOWLEDGMENT

We thank Dr. Roland Cooper (Old Dominion University, Norfolk, VA) for the anti-PfCRT antibody, our laboratory colleagues for helpful discussions, and Dr. Amrita Cheema and the proteomics core facility of Lombardi Cancer Center, Georgetown University Medical Center, for help with mass spectrometry. We also thank Dr. Sona Vasudevan, of the Protein Information Resource (PIR) at Georgetown University, for help in drawing Figure 10.

SUPPORTING INFORMATION AVAILABLE

Additional details as well as relevant NMR spectra, peak assignments, and HPLC spectra. This material is available free of charge via the Internet at http://pubs.acs.org.

REFERENCES

1. Fidock, D. A., Nomura, T., Talley, A. K., Cooper, R. A., Dzekunov, S. M., Ferdig, M. T., Ursos, L. M., Sidhu, A. B., Naudé, B., Deitsch, K. W., Su, X. Z., Wootton, J. C., Roepe, P. D., and Wellems, T. E. (2000) Mutations in the *P. falciparum* digestive vacuole transmembrane protein PfCRT and evidence for their role in chloroquine resistance. *Mol. Cell 6* (4), 861–871.
2. Cooper, R. A., Ferdig, M. T., Su, X. Z., Ursos, L. M., Mu, J., Nomura, T., Fujioka, H., Fidock, D. A., Roepe, P. D., and Wellems, T. E. (2002) Alternative mutations at position 76 of the vacuolar transmembrane protein PfCRT are associated with chloroquine resistance and unique stereospecific quinine and quinidine responses in Plasmodium falciparum. *Mol. Pharmacol. 61* (1), 35–42.
3. Sanchez, C. P., McLean, J. E., Rohrbach, P., Fidock, D. A., Stein, W. D., and Lanzer, M. (2005) Evidence for a pfcrt-associated chloroquine efflux system in the human malarial parasite *Plasmodium falciparum*. *Biochemistry 44* (29), 9862–9870.
4. Zhang, H., Paguio, M., and Roepe, P. D. (2004) The antimalarial drug resistance protein *Plasmodium falciparum* chloroquine resistance transporter binds chloroquine. *Biochemistry 43* (26), 8290–8296.
5. Bray, P. G., Mungthin, M., Hastings, I. M., Biagini, G. A., Saidu, D. K., Lakshmanan, V., Johnson, D. J., Hughes, R. H., Stocks, P. A., O'Neill, P. M., Fidock, D. A., Warhurst, D. C., and Ward, S. A. (2006) PfCRT and the trans-vacuolar proton electrochemical gradient: Regulating the access of chloroquine to ferriprotoporphyrin IX. *Mol. Microbiol. 62* (1), 238–251.
6. Bennett, T. N., Kosar, A. D., Ursos, L. M., Dzekunov, S., Singh Sidhu, A. B., Fidock, D. A., and Roepe, P. D. (2004) Drug resistance-associated pfCRT mutations confer decreased *Plasmodium falciparum* digestive vacuolar pH. *Mol. Biochem. Parasitol. 133* (1), 99–114.
7. Foley, M., Deady, L. W., Ng, K., Cowman, A. F., and Tilley, L. (1994) Photoaffinity labeling of chloroquine-binding proteins in *Plasmodium falciparum*. *J. Biol. Chem. 269* (9), 6955–6961.
8. Menting, J. G. T., Tilley, L., Deady, L. W., Ng, K., Simpson, R. J., Cowman, A. F., and Foley, M. (1997) The antimalarial drug,

chloroquine, interacts with lactate dehydrogenase from *Plasmodium falciparum*. *Mol. Biochem. Parasitol. 88* (1−2), 215–224.
9. Gligorijevic, B., Purdy, K., Elliott, D. A., Cooper, R. A., and Roepe, P. D. (2008) Stage independent chloroquine resistance and chloroquine toxicity revealed via spinning disk confocal microscopy. *Mol. Biochem. Parasitol. 159* (1), 7–23.
10. Zhang, H., Howard, E. M., and Roepe, P. D. (2002) Analysis of the antimalarial drug resistance protein PfCRT expressed in yeast. *J. Biol. Chem. 277* (51), 49767–49775.
11. Yang, J., Hodel, A., and Holman, G. D. (2002) Insulin and isoproterenol have opposing roles in the maintenance of cytosol pH and optimal fusion of GLUT4 vesicles with the plasma membrane. *J. Biol. Chem. 277* (8), 6559–6566.
12. Musial-Siwek, M., Rusch, S. L., and Kendall, D. A. (2007) Selective photoaffinity labeling identifies the signal peptide binding domain on SecA. *J. Mol. Biol. 365* (3), 637–648.
13. Gowda, A. S., Madhunapantula, S. V., Achur, R. N., Valiyaveettil, M., Bhavanandan, V. P., and Gowda, D. C. (2007) Structural basis for the adherence of *Plasmodium falciparum*-infected erythrocytes to chondroitin 4-sulfate and design of novel photoactivable reagents for the identification of parasite adhesive proteins. *J. Biol. Chem. 282* (2), 916–928.
14. Keana, J. F. W., and Cai, S. X. (1990) New reagents for photoaffinity labeling: Synthesis and photolysis of functionalized perfluorophenyl azides. *J. Org. Chem. 55* (11), 3640–3647.
15. Myers, M. C., Pokorski, J. K., and Appella, D. H. (2004) Peptide nucleic acids with a flexible secondary amine in the backbone maintain oligonucleotide binding affinity. *Org. Lett. 6* (25), 4699–4702.
16. Gligorijevic, B., Bennett, T. N., McAllister, R., Urbach, J., and Roepe, P. D. (2006) Spinning disk confocal microscopy of intraerythrocytic malarial parasites II: Quantification of digestive vacuolar volume. *Biochemistry 45* (41), 12411–12423.
17. Dufour, J. P., and Goffeau, A. (1980) Molecular and kinetic properties of the purified plasma membrane ATPase of the yeast *Schizosaccharomyces pombe*. *Eur. J. Biochem. 105* (1), 145–154.
18. Fritz, F., Howard, E. M., Hoffman, M. M., and Roepe, P. D. (1999) Evidence for altered ion transport in *Saccharomyces cerevisiae* overexpressing human MDR1 protein. *Biochemistry 38* (13), 4214–4226.
19. Safa, A. R., Glover, C. J., Meyers, M. B., Biedler, J. L., and Felsted, R. L. (1986) Vinblastine photoaffinity labeling of a high molecular weight surface membrane glycoprotein specific for multidrug-resistant cells. *J. Biol. Chem. 261* (14), 6137–6140.
20. Cornwell, M. M., Safa, A. R., Felsted, R. L., Gottesman, M. M., and Pastan, I. (1986) Membrane vesicles from multidrug-resistant human cancer cells contain a specific 150- to 170-kDa protein detected by photoaffinity labeling. *Proc. Natl. Acad. Sci. U.S.A. 83* (11), 3847–3850.
21. Safa, A. R. (1988) Photoaffinity labeling of the multidrug-resistance-related P-glycoprotein with photoactive analogs of verapamil. *Proc. Natl. Acad. Sci. U.S.A. 85* (19), 7187–7191.
22. Gilsdorf, J. S., Rebbeor, J. F., and Holohan, P. D. (1997) Evidence that the organic cation/H^+ exchanger in the brush border membrane of dog kidney is a 41-kDa protein. *J. Pharmacol. Exp. Ther. 280* (2), 1043–1050.
23. Black, M. E., Rechtin, T. M., and Drake, R. R. (1996) Effect on substrate binding of an alteration at the conserved aspartic acid-162 in herpes simplex virus type 1 thymidine kinase. *J. Gen. Virol. 77* (7), 1521–1527.
24. Chehade, K. A., Kiegiel, K., Isaacs, R. J., Pickett, J. S., Bowers, K. E., Fierke, C. A., Andres, D. A., and Spielmann, H. P. (2002) Photoaffinity analogues of farnesyl pyrophosphate transferable by protein farnesyl transferase. *J. Am. Chem. Soc. 124* (28), 8206–8219.
25. Joubert, S., Jossart, C., McNicoll, N., and De Léan, A. (2005) Atrial natriuretic peptide-dependent photolabeling of a regulatory ATP-binding site on the natriuretic peptide receptor-A. *FEBS J. 272* (21), 5572–5583.
26. Halmos, T., Turek, J. W., Le Breton, G. C., and Antonakis, K. (1999) Synthesis and biological characterization of sqbazide, a novel biotinylated photoaffinity probe for the study of the human platelet thromboxane A2 receptor. *Bioorg. Med. Chem. Lett. 9* (20), 2963–2968.
27. Cooper, R. A., Lane, K. D., Deng, B., Mu, J., Patel, J. J., Wellems, T. E., Su, X., and Ferdig, M. T. (2007) Mutations in transmembrane domains 1, 4 and 9 of the *Plasmodium falciparum* chloroquine resistance transporter alter susceptibility to chloroquine, quinine and quinidine. *Mol. Microbiol. 63* (1), 270–282.
28. Johnson, D. J., Fidock, D. A., Mungthin, M., Lakshmanan, V., Sidhu, A. B., Bray, P. G., and Ward, S. A. (2004) Evidence for a central role for PfCRT in conferring *Plasmodium falciparum* resistance to diverse antimalarial agents. *Mol. Cell 15* (6), 867–877.

BI8010658